CrossMark

LETTER

Hosking integral in non-helical Hall cascade

Axel Brandenburg [1,2,†]

[1]Nordita, KTH Royal Institute of Technology and Stockholm University, Hannes Alfvéns väg 12, SE-10691 Stockholm, Sweden

[2]Isaac Newton Institute for Mathematical Sciences, 20 Clarkson Road, Cambridge CB3 0EH, UK

The Hosking integral, which characterizes magnetic helicity fluctuations in subvolumes, is known to govern the decay of magnetically dominated turbulence. Here, we show that, when the evolution of the magnetic field is controlled by the motion of electrons only, as in neutron star crusts, the decay of the magnetic field is still controlled by the Hosking integral, but now it has effectively different dimensions than in ordinary magnetohydrodynamic (MHD) turbulence. This causes the correlation length to increase with time t like $t^{4/13}$ instead of $t^{4/9}$ in MHD. The magnetic energy density decreases like $t^{-10/13}$, which is slower than in MHD, where it decays like $t^{-10/9}$. These new analytic results agree with earlier numerical simulations for the non-helical Hall cascade.

---

1. Introduction

The X-ray emission from neutron stars during the first hundreds of years is believed to be powered by magnetic dissipation within their outer crusts (Gourgouliatos, Hollerbach & Archibald 2018). Since the ions are immobile in neutron star crusts, electric currents are transported by electrons alone (Cho & Lazarian 2009). Their velocity is $u = -J/en_e$, where $J = \nabla \times B/\mu_0$ is the current density, B is the magnetic field, e is the elementary charge, n_e is the electron density and μ_0 is the permeability. The evolution of B is then governed by the induction equation where the electromotive force $u \times B$ is given by $-J \times B/en_e$. The induction equation therefore takes the form (Goldreich & Reisenegger 1992)

$$\frac{\partial B}{\partial t} = \nabla \times \left(-\frac{1}{en_e} J \times B - \eta \mu_0 J \right), \qquad (1.1)$$

where η is the magnetic diffusivity. The $J \times B$ nonlinearity in this equation leads to a cascade toward smaller scales – similar to the turbulent cascade in hydrodynamic turbulence (Goldreich & Reisenegger 1992). This model is therefore referred to what is called the Hall cascade. There has been extensive work trying to quantify the amount

† Email address for correspondence: brandenb@nordita.org

of dissipation that occurs (Gourgouliatos, Wood & Hollerbach 2016; Gourgouliatos & Hollerbach 2018; Gourgouliatos, Hollerbach & Igoshev 2020; Igoshev, Popov & Hollerbach 2021; Anzuini *et al.* 2022). Idealized simulations in a Cartesian geometry resulted in power law scaling for the resistive Joule dissipation (Brandenburg 2020, hereafter B20). It depends on the typical length scale of the turbulence, the electron density, the magnetic field strength and the presence or absence of magnetic helicity. Denoting volume averages by angle brackets, the decay of the magnetic energy density $\mathcal{E} = \langle \boldsymbol{B}^2 \rangle / 2\mu_0$ with time t tends to follow power law behaviour, $\mathcal{E} \propto t^{-p}$, where the exponent p is smaller than in magnetohydrodynamic (MHD) turbulence. Here, $\langle \cdots \rangle$ denotes volume averaging over the spatial coordinates $\boldsymbol{x}$. In the helical case, it was found that $p = 2/5$, while for the non-helical case, B20 reported $p \approx 0.9$. The correlation length of the turbulence, ξ, increases with time like $\xi \propto t^q$, where $q = 2/5$ in the helical case, i.e. $q = p$, and $q \approx 0.3$ in the non-helical case. In the helical case, the exponent $2/5$ was possible to explain on dimensional grounds by noting that the magnetic field does not correspond to a speed (the Alfvén speed, as in MHD) with dimensions m s^{-1} in SI units, but to a diffusivity with dimensions m^2 s^{-1}.

The decay properties of the non-helical Hall cascade were not yet theoretically understood at the time. In the last one to two years, however, significant progress has been made in describing the decay of magnetically dominated turbulence, where a new conserved quantity has been identified, which is now called the Hosking integral (see Zhou, Sharma & Brandenburg (2022), for details regarding the naming). The purpose of the present paper is to propose the scaling of the Hall cascade under the assumption that it is governed by the constancy of the Hosking integral, which now has different dimensions than in MHD.

2. Hosking integral and scaling for the Hall cascade

The Hosking integral I_H is defined as the asymptotic limit of the magnetic helicity density correlation integral $\mathcal{I}_H(R)$ for scales R large compared with the correlation length of the turbulence, ξ, but small compared with the system size L. The original work on this integral is that by Hosking & Schekochihin (2021), who subsequently applied it to the magnetic field decay in the early universe (Hosking & Schekochihin 2022); see also Brandenburg, Kahniashvili & Tevzadze (2015) and Brandenburg & Kahniashvili (2017) for earlier work where inverse cascading of magnetically dominated non-helical turbulence was first reported. The function $\mathcal{I}_H(R)$ is given by

$$\mathcal{I}_H(R) = \int_{V_R} \mathrm{d}^3 r \langle h(\boldsymbol{x}) h(\boldsymbol{x} + \boldsymbol{r}) \rangle, \tag{2.1}$$

where V_R is the volume of a ball of radius R and $h = \boldsymbol{A} \cdot \boldsymbol{B}$ is the magnetic helicity density with $\boldsymbol{A}$ being the magnetic vector potential, so $\boldsymbol{B} = \nabla \times \boldsymbol{A}$. We recall that $\langle \cdots \rangle$ denotes averaging over $\boldsymbol{x}$. The function $\mathcal{I}_H(R)$ is thus the integral over the volume $V_R = 4\pi R^3 / 3$. For small R, it increases proportional to R^3, but for large R, it levels off. This is the value of R which determines the Hosking integral $I_H \equiv \mathcal{I}_H(R)$. In practice, it is chosen empirically and must still be small compared with the size of the domain; see Hosking & Schekochihin (2021) for various examples and Zhou *et al.* (2022) for a comparison of different computational techniques for obtaining $\mathcal{I}_H(R)$.

What matters for the Hall cascade is the fact that the dimensions of h are $[h] = [B]^2[x]$, and therefore the dimensions of $\mathcal{I}_H$ and I_H are

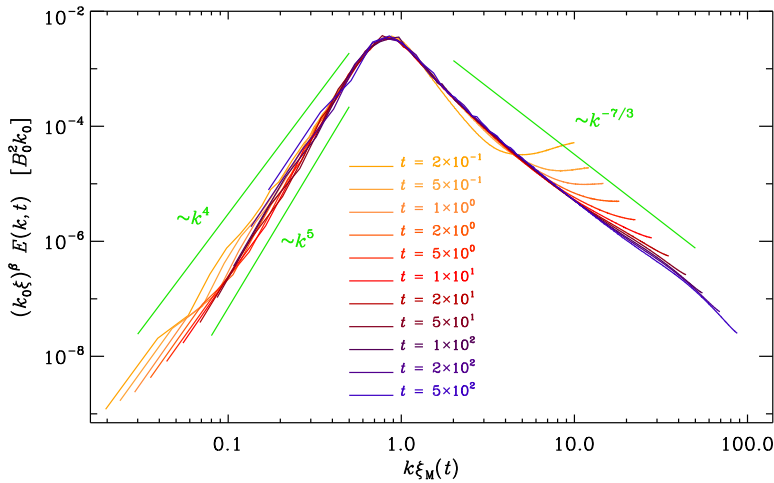$$[I_H] = [B]^4[x]^5. \tag{2.2}$$

FIGURE 1. Compensated spectra for Run B of B20, which corresponds to Run B1 in the present paper. Here, $\beta = 1.7$ has been used as the best empirical fit parameter.

However, as already noted in B20, using $e = 1.6 \times 10^{-19}$ As, $\mu_0 = 4\pi \times 10^{-7}$ T m A^{-1} and $n_e \approx 2.5 \times 10^{40}$ m^{-3} for neutron star crusts, we have $e n_e \mu_0 \approx 5 \times 10^{15}$ T s m^{-2}, and therefore

$$\frac{B}{e n_e \mu_0} = \frac{B}{5 \times 10^{15} \text{ T}} \frac{\text{m}^2}{\text{s}}, \tag{2.3}$$

which is why we say B has dimensions of m^2 s^{-1}.[1] Therefore, the dimensions of I_H are

$$[I_H] = [x]^{13}[s]^{-4}. \tag{2.4}$$

Thus, given that $I_H = $ const. in the limit of small magnetic diffusivity, a self-similar evolution must imply that all relevant length scales, and in particular the magnetic correlation length $\xi(t)$, must increase with time like $\xi \sim t^{4/13}$. Since $4/13 \approx 0.31$, this is indeed close to the behaviour $\xi \sim t^q$ with $q \approx 0.3$ found in § 3.2 of B20 (their Run B), as already highlighted in the introduction of the present paper.

To demonstrate that the energy spectra $E(k, t)$ at different times are indeed self-similar, we collapse them on top of each other by plotting them versus $k\xi(t)$. Here, $\xi(t) = \mathcal{E}^{-1} \int k^{-1} E(k, t) \, dk$ is the weighted integral of k^{-1}, where the spectra are normalized such that $\int E(k, t) \, dk = \mathcal{E}(t)$ is the magnetic energy density. This ensures that the maxima of $E(k\xi)$ are always approximately near $k\xi(t) = 1$. In addition, we must also compensate for the decay in amplitude by multiplying the spectra by a time-dependent function, e.g. $\xi(t)^\beta$, where β is a suitable exponent, so that the compensated spectra all have the same height. In this way, we find a universal spectral function by plotting

$$[\xi(t)]^\beta E(k\xi(t), t) \equiv \phi(k\xi(t)). \tag{2.5}$$

As an example, we show in figure 1 the compensated spectra for Run B of B20, which we discuss in more detail below. At this point, we just note that these were solutions to (1.1), where the initial condition consists of a non-helical magnetic field with a spectrum

---

[1]In MHD, by comparison, the ion density ρ is a relevant quantity. Using $\rho = 10^3$ kg m^{-3} for solar surface plasmas, and the identity 1 T = 1 kg s^{-2}A^{-1}, we have $\mu_0 = 4\pi \times 10^{-7}$ T^2 s^{2}m kg^{-1}, and therefore $\rho\mu_0 \approx 3.5 \times 10^{-2}$ T s m^{-1}, or $B/\sqrt{\rho_0\mu_0} = (B/3.5 \times 10^{-2}$ T) m s^{-1}, which is why we say that, in MHD, B has dimensions of ms^{-1}.

$E(k) \propto k^4$ for $k \ll k_0$, with k_0 being the initial peak wavenumber. For $k \gg k_0$, we assume a decaying spectrum, here with $E(k) \propto k^{-5/3}$, although this particular choice of the exponent was not important. After some time, the spectral slopes of both subranges change: at small k, the spectrum steepens from k^4 to k^5. Beyond the peak, it falls off with a $k^{-7/3}$ inertial range, as was already found by Biskamp, Schwarz & Drake ([1996](#)).

To determine the theoretically expected value of β, we invoke the condition that the compensated spectra be invariant under rescaling, $t \to \tau t'$, $\boldsymbol{x} \to \tau^q \boldsymbol{x}'$, where τ is an arbitrary scaling factor. We recall that the dimensions of $E(k, t)$ are $[x]^5[t]^{-2}$, so rescaling yields a factor τ^{5q-2}. In addition, expressing E' in terms of its universal spectral function $\phi(k\xi)$, the factor ξ^β on the left-hand side of (2.5) produces a factor $\xi^{-\beta}$ on the right-hand side of (2.5), and therefore, after rescaling, a $\tau^{-\beta q}$ factor, i.e.

$$E(k) \to \tau^{5q-2}E'(k) \propto \xi(t)^{-\beta}\tau^{-\beta q}\phi(k\xi). \tag{2.6}$$

Therefore, $5q - 2 = -\beta q$ must be satisfied in order that the compensated spectra remain invariant under rescaling. Thus, $\beta = 2/q - 5$, as already found in B20. Inserting now $q = 4/13$ yields $\beta = 3/2$. The total magnetic energy density is therefore

$$\mathcal{E} = \int \xi^{-\beta}\phi(k\xi)\,\mathrm{d}k = \xi^{-(\beta+1)}\int \phi(k\xi)\,\mathrm{d}(k\xi) \propto t^{-(\beta+1)q}, \tag{2.7}$$

and since $\mathcal{E} \propto t^{-p}$, we have[2] $p = (\beta + 1)q$. Using $\beta = 2/q - 5$, we have $p = 2(1 - 2q)$; see (28) of B20. For $q = 4/13 \approx 0.31$, we have $p = 2(1 - 8/13) = 10/13 \approx 0.78$, which is not quite as close to the value reported in B20 as that of q, but this could be ascribed to the lack of scale separation and also the magnetic field no longer being strong enough so that the Lundquist number,[3]

$$\mathrm{Lu} = B_{\mathrm{rms}}/en_e\mu_0\eta, \tag{2.8}$$

is no longer in the asymptotic regime. This also resulted in the empirical value of β being slightly larger than the theoretical one, as we will see next.

3. Comparison with simulations for different diffusivities

In B20, various simulations of the Hall cascade have been presented, including forced and decaying simulations, helical and non-helical ones, with constant and time-varying magnetic diffusivities, with and without stratification, etc. The main purpose of that work was to understand the dissipative losses that would lead to resistive heating in the crust of a neutron star. One of those simulations is particularly relevant for the present paper: his Run B, which had a relatively strong initial magnetic field, no helicity, large scale separation and a magnetic diffusivity that decreased with time in a power law fashion, allowing the simulation to retain a higher Lundquist number as the magnetic field decreases.

In the present paper, we analyse his Run B, which is here called Run B1. It is actually a new run, because we now have calculated the Hosking integral during run time. We also compare with another run (Run B2), where we decreased the magnetic diffusivity by a

---

[2]An equivalent, but conceptually simpler route to the $t^{-10/13}$ decay law, suggested by D.N. Hosking (private communication), is to use (1.1) to argue that the timescale t_{dec} for magnetic decay is proportional to ξ^2/B. Since t_{dec} is proportional to t for self-similar decay, we get, using $\xi^5 B^4 = [B^2(\xi^2/B)^{10/13}]^{13/4} = (B^2 t^{10/13})^{13/4} = \mathrm{const.}$, the scaling $B^2 \propto t^{-10/13}$. The difference between MHD and Hall cascade is that, in the former, t_{dec} is proportional to ξ/B, but $\propto \xi^2/B$ in the latter.

[3]Note that, unlike the case of MHD, in the present case of Hall cascade, no wavenumber factor enters in the definition of the Lundquist number.

Run	Lu	$t_1/[t]$	$t_2/[t]$	$\tilde{\eta}$	$\tilde{B}_{rms}$	$\tilde{\epsilon}$	p	q	β	p_H
B1	650	0.2	500	0.024	600	3×10^6	0.8 ± 0.1	0.3 ± 0.1	1.7 ± 0.1	0.16
B2	1300	3	200	0.011	700	6×10^6	0.78 ± 0.05	0.31 ± 0.05	1.6 ± 0.05	0.11

TABLE 1. Summary of runs discussed in this paper.
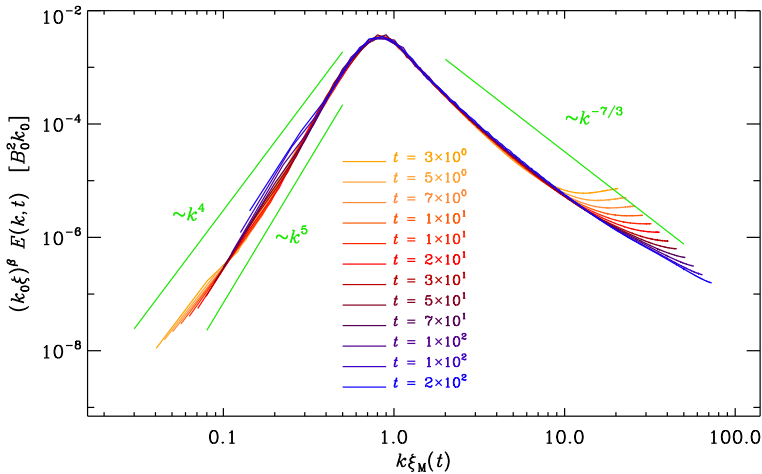
FIGURE 2. Compensated spectra for Run B2.

factor of two. As in B20, η is assumed to decrease with time proportional to $t^{-3/7}$. We kept, however, the same resolution of 1024^3 mesh points for both runs, but we must keep in mind that this can lead to artefacts resulting from a poorly resolved diffusive subrange for Run B2.

In table 1, we compare several characteristic parameters: the start and end times, t_1 and t_2, respectively, of the interval for which averaged data have been accumulated, non-dimensional measures of the magnetic diffusivity, the magnetic field strength and the dissipation, $\tilde{\eta}$, $\tilde{B}_{rms}$ and $\tilde{\epsilon}$, respectively, and the instantaneous scaling exponents p, q and β. For $\tilde{\eta}$, $\tilde{B}_{rms}$ and $\tilde{\epsilon}$, we compute the following time-averaged ratios:

$$\tilde{\eta} \equiv \langle t\eta/\xi^2 \rangle_t, \quad \tilde{B}_{rms} \equiv \langle B_{rms}/(en_e\mu_0\eta) \rangle_t, \quad \text{and} \quad \tilde{\epsilon} \equiv \langle \epsilon/(e^2 n_e^2 \mu_0 \eta^3/\xi^2) \rangle_t, \quad (3.1a\text{–}c)$$

where $\xi(t) = \mathcal{E}^{-1} \int k^{-1} E(k, t) \, dk$ is the correlation length and $\epsilon = \eta\mu_0\langle J^2 \rangle$ is the magnetic dissipation with $\eta = \eta(t)$, as noted above. These were also computed in B20. Time is given in diffusive units, $[t] = (\eta k_0^2)^{-1}$. In the runs of series B of B20, the value of k_0 is 180 times larger than the lowest wavenumber $k_1 \equiv 2\pi/L$ of our cubic domain of size L^3.

It turns out that a lower resistivity is important for obtaining the expected scaling. We therefore now consider Run B2, where Lu ≈ 1300. The result is shown in figure 2, where we used $\beta = 1.6$ as the best fit, which is still slightly larger than the expected value of 3/2, but it goes in the right direction. Therefore, we show in figure 2 the resulting compensated spectra for Run B2, where the magnetic diffusivity is half that of Run B1 and Lu is now twice as large a before; see table 1. We use the PENCIL CODE (Pencil Code Collaboration *et al.* 2021) and, in both cases, we use a resolution of 1024^3 mesh points.
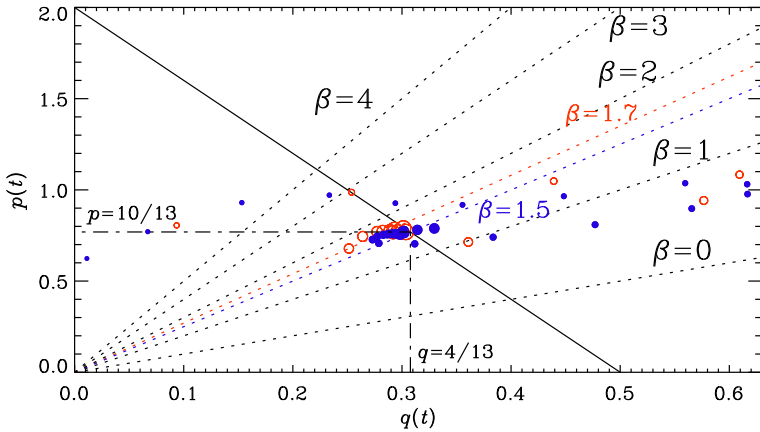
FIGURE 3. The *pq* diagrams for Runs B1 (open red symbols) and B2 (closed blue symbols).
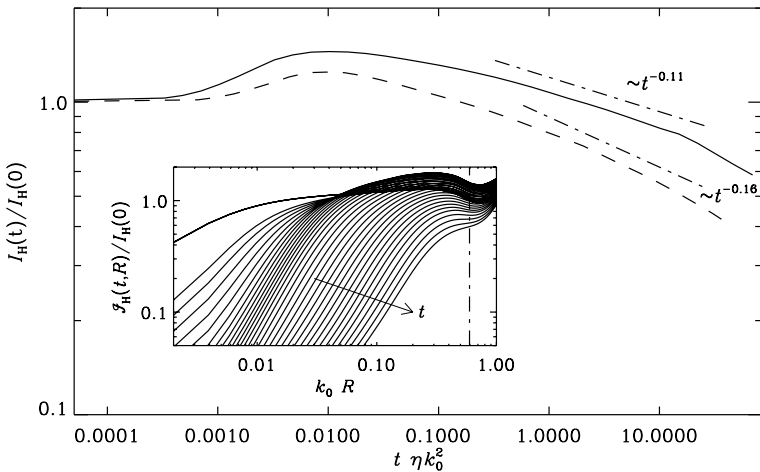Larger symbols denote later times.

FIGURE 4. Evolution of $I_H(t)$, showing first a slight increase and then a decline proportional to $t^{-0.16}$ for Run B1 and proportional to $t^{-0.11}$ for Run B2. The inset shows the evolution of $\mathcal{I}_H(R; t)$ as a function of R for increasing values of t (indicated by the arrow) for Run B2. The abscissae of the main plot and the inset are normalized by ηk_0^2 and k_0, respectively.

Another comparison between Runs B1 and B2 is shown in figure 3, where we compare their evolution in the *pq* diagram. While Run B1 clearly evolves along the $\beta \approx 1.7$ line, Run B2 tends to be closer to the $\beta \approx 3/2$ line. Note also that both runs settle near the $p = 2(1 - 2q)$ self-similarity line (B20), although we begin to see departures near the end of the run, which is due to the finite size of the domain.

Finally, we show in figure 4 the scalings of $I_H(t)$, where we see that the decay exponent $p_H \equiv -d \ln I_H / d \ln t$ is approximately $p_H \approx 0.16$ for Run B1 and approximately 0.11 for Run B2. Earlier work by Zhou *et al.* (2022) showed that p_H decreases as the Lundquist number increases, and is, in MHD, approximately 0.2 for Lu $\approx 10^3$, and decreases to $p_H \approx 0.01$ for Lu $\approx 4 \times 10^7$. Such large values can currently only be obtained with magnetic hyper-diffusivity (Hosking & Schekochihin 2021; Zhou *et al.* 2022), but this has not been attempted in the present work.

MHD	$[B] = [x]/[t]$	$[\langle h \rangle] = [x]^3/[t]^2$	$q = 2/3$ (helical)
		$[I_H] = [x]^9/[t]^4$	$q = 4/9$ (non-hel)
	$[E(k,t)] = [x]^3[t]^{-2}$	$\beta = 2/q - 3$	$\beta = 2 \cdot 9/4 - 3 = 3/2$
		$p = 2(1-q)$	$p = 2(1 - 4/9) = 10/9$
Hall	$[B] = [x]^2/[t]$	$[\langle h \rangle] = [x]^5/[t]^2$	$q = 2/5$ (helical)
		$[I_H] = [x]^{13}/[t]^4$	$q = 4/13$ (non-hel)
	$[E(k,t)] = [x]^5[t]^{-2}$	$\beta = 2/q - 5$	$\beta = 2 \cdot 13/4 - 5 = 3/2$
		$p = 2(1-2q)$	$p = 2(1 - 2 \cdot 4/13) = 10/13$

TABLE 2. Comparison of the scalings for MHD and the Hall cascade.

As already noted by Zhou *et al.* (2022), there is an initial increase in $I_H(t)$. This is explained by the fact that the magnetic field obeys Gaussian statistics initially, but not during the later evolution. The inset shows the R dependence of $\mathcal{I}_H(R; t)$ for different t. The relevant value of R is deemed to be at the location where the local slope of $\mathcal{I}_H(R)$ is minimum at late times.

4. Conclusion

The present work has highlighted the power of dimensional arguments, which were here applied to the case of the Hall cascade without helicity, where the magnetic field is naturally represented as a quantity with units of a magnetic diffusivity. The magnetic helicity density has units of $m^5\,s^{-2}$ and the Hosking integral has units of $m^{13}s^{-4}$, which yields $q = 4/13$, $\beta = 3/2$ and $p = 10/13$. Comparing with standard MHD, where the magnetic field has units of $m\,s^{-1}$, our exponents p and q are now smaller, but β is still the same in both cases; see table 2 for a comparison between Hall cascade and MHD. The empirically determined value of β is somewhat larger, but this can be explained by finite scale separation and small Lundquist numbers.

The decay properties of the Hall cascade are important in understanding resistive heating in neutron stars while producing at the same time larger scale magnetic fields at a certain speed through inverse cascading (B20). Such simulations have already been done in a spherical geometry (Gourgouliatos *et al.* 2020), but the magnetic field in those simulations did not yet exhibit clear forward or inverse cascading. This is presumably due to their initial magnetic field being strongly localized at intermediate length scales. Using an initial broken power law, as done here, would help producing the expected forward or inverse cascadings, but this may also require much larger resolution than what is currently possible. Similarly, of course, the values of n_e and η are depth dependent in real neutron stars, but the work of B20 showed that this did not affect the scaling behaviour of the magnetic decay. Therefore, the importance of the Hosking integral may well carry over to real neutron stars.

The possible role of reconnection in the Hall cascade remains an open question. In the case of MHD, reconnection has been discussed extensively by Hosking & Schekochihin (2021), making reference to earlier work by Zhou *et al.* (2019), Zhou, Loureiro & Uzdensky (2020) and Bhat, Zhou & Loureiro (2021). Also, in the Hall cascade there is the possibility that the decay of $\mathcal{E}$ could be slowed down in an intermediate range of values of the Lundquist number. As shown in Zhou *et al.* (2022), this could lead to a termination line in the *pq* diagrams that is different from the $p = 2(1 - 2q)$ self-similarity line discussed

here. At the moment, however, there is no compelling evidence for deviations of the solutions from the self-similarity line.

Declaration of interests

The authors declare no conflict of interest.

Data availability statement

The data that support the findings of this study are openly available on Zenodo at doi:10.5281/zenodo.7357799 (v2022.11.24). All calculations have been performed with the PENCIL CODE (Pencil Code Collaboration *et al.* 2021); doi:10.5281/zenodo.3961647.

REFERENCES

ANZUINI, F., MELATOS, A., DEHMAN, C., VIGANÒ, D. & PONS, J.A. 2022 Thermal luminosity degeneracy of magnetized neutron stars with and without hyperon cores. *Mon. Not. R. Astron. Soc.* **515** (2), 3014–3027. arXiv:2205.14793.

BHAT, P., ZHOU, M. & LOUREIRO, N.F. 2021 Inverse energy transfer in decaying, three-dimensional, non-helical magnetic turbulence due to magnetic reconnection. *Mon. Not. R. Astron. Soc.* **501** (2), 3074–3087. arXiv:2007.07325.

BISKAMP, D., SCHWARZ, E. & DRAKE, J.F. 1996 Two-dimensional electron magnetohydrodynamic turbulence. *Phys. Rev. Lett.* **76** (8), 1264–1267.

BRANDENBURG, A. 2020 Hall cascade with fractional magnetic helicity in neutron star crusts. *Astrophys. J.* **901** (1), 18. arXiv:2006.12984.

BRANDENBURG, A. & KAHNIASHVILI, T. 2017 Classes of hydrodynamic and magnetohydrodynamic turbulent decay. *Phys. Rev. Lett.* **118** (5), 055102. arXiv:1607.01360.

BRANDENBURG, A., KAHNIASHVILI, T. & TEVZADZE, A.G. 2015 Nonhelical inverse transfer of a decaying turbulent magnetic field. *Phys. Rev. Lett.* **114** (7), 075001. arXiv:1404.2238.

CHO, J. & LAZARIAN, A. 2009 Simulations of electron magnetohydrodynamic turbulence. *Astrophys. J.* **701** (1), 236–252. arXiv:0904.0661.

GOLDREICH, P. & REISENEGGER, A. 1992 Magnetic field decay in isolated neutron stars. *Astrophys. J.* **395**, 250.

GOURGOULIATOS, K.N. & HOLLERBACH, R. 2018 Magnetic axis drift and magnetic spot formation in neutron stars with toroidal fields. *Astrophys. J.* **852** (1), 21. arXiv:1710.01338.

GOURGOULIATOS, K.N., HOLLERBACH, R. & ARCHIBALD, R.F. 2018 Modelling neutron star magnetic fields. *Astron. Geophys.* **59** (5), 5.37–5.42.

GOURGOULIATOS, K.N., HOLLERBACH, R. & IGOSHEV, A.P. 2020 Powering central compact objects with a tangled crustal magnetic field. *Mon. Not. R. Astron. Soc.* **495** (2), 1692–1699. arXiv:2005.02410.

GOURGOULIATOS, K.N., WOOD, T.S. & HOLLERBACH, R. 2016 Magnetic field evolution in magnetar crusts through three-dimensional simulations. *Proc. Natl Acad. Sci.* **113** (15), 3944–3949. arXiv:1604.01399.

HOSKING, D.N. & SCHEKOCHIHIN, A.A. 2021 Reconnection-controlled decay of magnetohydrodynamic turbulence and the role of invariants. *Phys. Rev.* X **11** (4), 041005. arXiv:2012.01393.

HOSKING, D.N. & SCHEKOCHIHIN, A.A. 2022 Cosmic-void observations reconciled with primordial magnetogenesis. arXiv:2203.03573.

IGOSHEV, A.P., POPOV, S.B. & HOLLERBACH, R. 2021 Evolution of neutron star magnetic fields. *Universe* **7** (9), 351. arXiv:2109.05584.

PENCIL CODE COLLABORATION, *et al.* 2021 The Pencil Code, a modular MPI code for partial differential equations and particles: multipurpose and multiuser-maintained. *J. Open Source Softw.* **6** (58), 2807. arXiv:2009.08231.

ZHOU, M., BHAT, P., LOUREIRO, N.F. & UZDENSKY, D.A. 2019 Magnetic island merger as a mechanism for inverse magnetic energy transfer. *Phys. Rev. Res.* **1** (1), 012004. arXiv:1901.02448.

ZHOU, M., LOUREIRO, N.F. & UZDENSKY, D.A. 2020 Multi-scale dynamics of magnetic flux tubes and inverse magnetic energy transfer. *J. Plasma Phys.* **86** (4), 535860401. arXiv:2001.07291.

ZHOU, H., SHARMA, R. & BRANDENBURG, A. 2022 Scaling of the Hosking integral in decaying magnetically dominated turbulence. *J. Plasma Phys.* **88** (6), 905880602. arXiv:2206.07513.